

# Computer simulation studies of structure characteristics of ordered mesoporous carbons and its naphthalene adsorption performance

Keliang Wang<sup>1</sup>, Mingli Fu<sup>2</sup>, Junliang Wu<sup>2</sup>, Guangying Zhou<sup>3</sup>, Daiqi Ye<sup>2\*</sup>

<sup>1</sup> Guangdong Polytechnic of Environmental Protection Engineering, Guangdong 528216, China

<sup>2</sup> School of Environment and Energy, South China University of Technology, Guangzhou 510006, China

<sup>3</sup> School of Chemistry and Environment, South China Normal University, Guangzhou 510006, China

## Abstract:

We could draw some valuable conclusions about adsorption capacity, adsorption isotherm, adsorption kinetics, adsorption thermodynamics by naphthalene adsorption experiments, but the experiments could not tell us directly what the adsorption location and adsorption state are exactly on the surface of OMCs. Actually, we still don't know the microscopic structure of OMCs very well because of the restriction of characterization technology, human factor and experimental conditions. However, molecular simulation technology could make up the disadvantages. In the work, Grand Canonical Monte Carlo method was performed for the first time to simulate the naphthalene adsorption behavior in OMCs structure model. The atomic structure model of OMCs was built firstly by using molecular modeling technique and was characterized by calculating the accessible solvent surface area, total pore volume, and small-angle X-ray diffraction patterns. The calculated results showed that the structure model of OMCs was reasonable and the structure characteristic was in agreement with experimental data. The adsorption isotherm curve is of type Langmuir IV, which was typical characteristic of ordered mesoporous materials. Also, adsorption isotherm curve revealed that the adsorption capacity of naphthalene on OMCs increased to a balance gradually, and the maximum adsorption capacity of naphthalene was 105.4 mg g<sup>-1</sup>. Additionally, the adsorption state of naphthalene were observed that from monolayer to multilayer in the mesopores with the increasing of number of naphthalene molecules.

This work deepened the understanding of the adsorption state of naphthalene for OMCs on mesoscopic level. It also demonstrated that the GCMC method is effective for studying the adsorption process and gives useful guidance on research of structure-activity relationship and

---

\*Corresponding author phone: +86 20 39380516; fax: +86 20 39380518; e-mail address:

[cedqye@scut.edu.cn](mailto:cedqye@scut.edu.cn)

34 performance prediction of the carbon material.

35 **Keywords:** Grand Canonical Monte Carlo; Ordered mesoporous carbons; Adsorption;  
36 Naphthalene.

37

## 38 INTRODUCTION

39 Polycyclic aromatic hydrocarbons (PAHs), known as one of the persistent organic pollutants,  
40 which have threatened people health and atmospheric environment seriously (International  
41 Agency for Research on Cancer, 1983; Carcinogen Assessment Group, 1985; Ministry of  
42 Environment and Energy, 1997). PAHs typically disperse from urban and suburban non-point  
43 sources through road run-off, sewage, and atmospheric circulation and subsequent deposition of  
44 particulate air pollution due to their volatility and reactivity (Lee *et al.*, 1993; Sloss *et al.*, 1995;  
45 Mastral *et al.*, 1999; Hylland *et al.*, 2006). Therefore, adsorption is one of the most important  
46 methods to remove PAHs effectively (Gerde *et al.*, 1989; Hart *et al.*, 1994; Dachs *et al.*, 2000;  
47 Cheng *et al.*, 2008).

48 Ordered mesoporous carbons (OMCs) have attracted great attention because of their  
49 interesting applications in many fields recently, especially in adsorption, catalysis, separation,  
50 and energy storage/conversion devices (Galo *et al.*, 2002; Schrüth *et al.*, 2003; Guo *et al.*, 2005;  
51 Minchev *et al.*, 2005; Taguchi *et al.*, 2005; Lee *et al.*, 2006; Li *et al.*, 2006; Lu *et al.*, 2006; Wang  
52 *et al.*, 2013). Their utility for these applications could be attributed to ordered cubic or hexagonal  
53 frameworks, regulated pore sizes, narrow mesopore size distributions, high specific surface areas  
54 and large pore volumes. Therefore, the adsorption performance of OMCs for gaseous molecules  
55 is very well. However, most research focused on the adsorption capacity, adsorption isotherm,  
56 adsorption kinetics and adsorption thermodynamics (Zhou *et al.*, 2005; Saha *et al.*, 2010; Saini *et al.*,  
57 2010; Wang *et al.*, 2013), and the experimental results could not tell us directly what the  
58 adsorption location and adsorption state are exactly on the surface of OMCs. Actually, we still  
59 don't know the microscopic structure of OMCs very well because of the restriction of  
60 characterization technology, human factor and experimental conditions.

61 Based on precise theoretical models for accurate theoretical calculation, the molecular  
62 simulation technique could be helpful for tackling the problem mentioned above. Grand

63 Canonical Monte Carlo (GCMC) method has been applied successfully in many fields, such as  
64 environment, material, adsorption and separation. The simulation results were proved that the  
65 GCMC method was a powerful and effective approach to probe the molecular adsorption action  
66 in mesoporous materials (Chen *et al.*, 2000; Sun *et al.*, 2009; Zhang *et al.*, 2012) and could be the  
67 necessary complement for the experimental approach.

68 In the work, GCMC method was performed for the first time to simulate the naphthalene  
69 adsorption behavior in OMCs. The atomic structure model of OMCs was built firstly by utilizing  
70 molecular modeling technique and was characterized by calculating the accessible solvent surface  
71 area, total mesopore volume and small-angle X-ray diffraction pattern. Additionally, the  
72 adsorption capacity and the adsorption state of naphthalene in OMCs were simulated. This work  
73 could deepen the understanding of the adsorption performance of naphthalene in OMCs on  
74 mesoscopic level, and the results could provide some valuable information for further research on  
75 structure-activity relationship, performance prediction of the carbon material and the removal of  
76 PAHs effectively.

## 77 **COMPUTATIONAL DETAILS**

78 The commercial software package Materials Studio (MS), developed by Accelrys in the  
79 USA, was applied in the simulations.

### 80 **OMCs Structure Model**

81 The atomic structure model of OMCs was built by utilizing Materials Visualizer module of  
82 MS, and the process was summarized as follows: Firstly, OMCs were consisted of amorphous  
83 carbon, so the unit cell of amorphous carbon was imported from the database of MS, and a  $5 \times 3 \times 2$   
84 supercell ( $10.7\text{nm} \times 6.4\text{nm} \times 4.2\text{nm}$ ) was built by the unit cell, the mesoporous size (diameter=4nm)  
85 of OMCs was determined based on the experimental results obtained by Wang *et al.* (Wang *et al.*,  
86 2012), for which the adsorption performance was the best under the experimental condition. The  
87 carbon atoms, which were inside the selected 4nm mesoporous pore diameter of the supercell,  
88 were removed, then the produced vacant bonds were not saturated with hydrogen atoms because  
89 the influence could be neglected after theoretical calculation. Finally, the atomic structure model  
90 of OMCs was built by applying P1 symmetry of the periodical boundary conditions, and the

91 synthesis process diagram was showed in Fig.1.

92

### 93 **Molecular dynamic (MD) simulation**

94 The Forcite module of MS was applied in the MD simulations. The geometry optimization  
95 of the OMCs structure model was performed firstly using periodical boundary conditions to avoid  
96 any arbitrary boundary effects in the simulation process. The COMPASS Force Field was  
97 employed and the charges in the electrostatic scalar potential format can be assigned to the  
98 calculated values during the geometry optimization process, and the structure of OMCs was  
99 equilibrated to obtain the minimum energy configuration at 298 K and NVT ensemble. A step  
100 size of 1 fs and total simulation time of 20 ps were chosen, respectively. Then, the entire structure  
101 model was equilibrated for 120 ps in NVE dynamics and frame output every 100 steps.

102

### 103 **Grand Canonical Monte Carlo (GCMC) simulation**

104 For predicting the phase equilibrium of adsorption, the GCMC simulation could be one of  
105 the most common techniques (Allen *et al.*, 1980; Fan *et al.*, 2017). It was applied usually to  
106 simulate the equilibrium of collection of adsorbate in a pore structure at constant chemical  
107 potential, volume, and temperature (or pressure). Because the chemical potential will get  
108 equilibrium under a reaction condition, we could simulate the adsorption characterization of  
109 naphthalene in OMCs in this work. The GCMC simulations of naphthalene adsorption in OMCs  
110 were carried out by the Sorption module of MS package applying for Metropolis method. The  
111 Metropolis algorithm, COMPASS force field and basis set were applied to research the adsorption  
112 performance of naphthalene after MD simulation with periodical boundary condition. In this  
113 work, the adsorption system was equilibrated for  $1 \times 10^5$  GCMC steps at 393K under the relative  
114 pressure range from 0 to 1 during the calculation. The electrostatic summation method was Ewald  
115 & Group, cutoff distance was 1.5nm, and the simulation data were collected for another  $1 \times 10^5$   
116 GCMC steps during the calculation to get the final adsorption structure, adsorption state and the  
117 adsorption capacity.

118

## 119 **RESULTS AND DISCUSSION**

120 **Structure details**

121 The structure model of OMCs after geometry optimization was showed in Fig. 2A, which  
122 was showed in ball and stick model, and the mesopore size was 4 nm and the lattice parameters  
123 were 10.7nm×6.4nm×4.2nm, respectively. The 3×3×1 supercell structure of OMCs was given in  
124 Fig. 2B. It revealed that the supercell structure obtained exhibited well ordered 2D-hexagonal  
125 structures, and the structures observed from parallel direction of channel were similar with the  
126 images of OMCs viewed along the (110) direction by TEM, which suggested that the simulation  
127 results were in good agreement with the experimental results (Wang *et al.*, 2012).

128 The atom volume and surface tools of MS were applied to calculate the accessible solvent  
129 surface area of the OMCs model, and the simulation results were showed in Fig. 3. This figure  
130 presented that the wall thickness, total mesopore volume and surface area were 2.3nm, 0.15cm<sup>3</sup>/g  
131 and 334m<sup>2</sup>/g, respectively. Additionally, the pore structure parameters of OMCs obtained by  
132 structure model are compared with the experimental data (Wang *et al.*, 2012), which were listed  
133 in the Table 1. It indicated that the mesopore sizes of them were same. However, the wall  
134 thickness, the accessible solvent surface area and the total mesopore volume were less than those  
135 of the experimental data. The decrease was probably because that structure units of OMCs were  
136 assumed perfect crystal during the process of simulation calculation. However, for realistic  
137 structure of OMCs, there are still some structural defects, impurity, surface coarseness, or pore  
138 wall thickness, which result in the simulation results are not in accord with the real structure fully.  
139 Additionally, there were a lot of pores, which sizes were less than 4nm, produced during the  
140 experimental preparation process of OMCs, the pore sizes distribution of experimental samples  
141 were concentrated in a relatively wider sizes range than simulation results. So these results  
142 mentioned above indicated that the model structure of OMCs still need further modification or  
143 optimization for the purpose of obtaining more accurate simulation results in subsequent research.  
144 Actually, it was normal and permitted that there were some difference between simulation results  
145 and experiment results, and the difference did not affect the simulation results reliability of the  
146 OMCs structure. Therefore, the simulation results demonstrated that structure model kept the  
147 typical structure characteristics of OMCs, and the structure model was reasonable and reliable.

148

## 149 **X-ray diffraction (XRD) analysis**

150 In order to investigate the structure characteristic of OMCs clearly, the Reflex module of MS  
151 was performed to simulate the small-angle XRD, and the XRD pattern was illustrated in Fig. 4.  
152 The Figure revealed three well resolved peaks, which were indexed to the (100), (110), and (200)  
153 diffraction peaks of a space group P6mm hexagonal structure (Liu *et al.*, 2006; Wang *et al.*, 2012).  
154 The values of interplanar spacing (d) were 5.48nm, 3.19nm and 2.74nm, respectively. Their ratios  
155 corresponded to 1:  $(1/\sqrt{3})$ : (1/2) (Trick *et al.*, 1995), which indicated that the OMCs had well-  
156 ordered 2D hexagonal structure. It suggested that the simulation results fit the experimental  
157 results very well (Wang *et al.*, 2012).

## 158 **Naphthalene adsorption**

159 The adsorption isotherm indicated the partition of adsorbate between gas and adsorbent at  
160 equilibrium. To study the adsorption capacity of OMCs at 393 K, the adsorption isotherm for  
161 naphthalene in the structure model of OMCs was calculated by GCMC, and the simulated result  
162 was showed in Fig. 5. The adsorption isotherm curve illustrated that the adsorption capacity of  
163 OMCs increased to a balance gradually when the relative pressure is increasing, and the  
164 maximum adsorption capacity was shown to reach up to 105.4mg/g. Additionally, the adsorption  
165 isotherm is of type Langmuir IV, which was the characteristic adsorption curve of mesoporous  
166 materials (Febrianto *et al.*, 2009; Zeng *et al.*, 2016), and the adsorption isotherm revealed that it  
167 was monolayer adsorption at lower pressure region ( $p/p_0 < 0.4$ ) and was multilayer adsorption at  
168 higher pressure region ( $p/p_0 > 0.4$ ).

169 After  $5 \times 10^5$  GCMC steps were performed, structures and density distribution of  
170 naphthalene in OMCs were recorded and showed at relative pressure level of 0, 0.2, 0.6 and 1.0  
171 in Fig. 6. The simulation results showed that there was almost not any naphthalene molecule was  
172 adsorbed in the OMCs under the relative pressure of 0 (Fig. 6(a)). Then, there were much more  
173 naphthalene molecules were adsorbed with the increase of relative pressure from 0.2 to 0.6, and  
174 the adsorption was from monolayer adsorption to multilayer adsorption gradually. Finally, the  
175 mesopore was filled fully with naphthalene molecules (Fig. 6(d)).

176 Additionally, the adsorption process could still was observed directly and clearly in Fig.7.  
177 The adsorption state of naphthalene were simulated that from monolayer to multilayer in the

178 mesopores with the increasing of number of naphthalene molecules, which corresponded with the  
179 simulation results in Fig. 6.

## 180 **CONCLUSIONS**

181 In the work, GCMC method was performed for the first time to simulate the naphthalene  
182 adsorption behavior in the OMCs. The structure model of OMCs on atomistic level was built  
183 firstly by using molecular modeling technique. Additionally, the total mesopore volume, surface  
184 area and small-angle XRD are calculated to analyze the structural characterization of the OMCs  
185 atomic model. The calculated results showed that the structure model of OMCs was reasonable  
186 and reliable, and the structure characteristic was corresponded with experimental results. The  
187 adsorption isotherm curve is of type Langmuir IV, which was considered as typical adsorption  
188 characteristic isotherm of mesoporous material. Also, the adsorption isotherm curve revealed that  
189 the adsorption capacity of naphthalene on OMCs increased to a balance gradually when the  
190 relative pressure increased from 0 to 1.0, and the maximum adsorption capacity is shown to reach  
191 up to 105.4mg/g. Additionally, the adsorption state of naphthalene were observed that from  
192 monolayer to multilayer in the mesopores with the increasing of number of naphthalene  
193 molecules. However, there is still some difference between experimental results and simulation  
194 results, which could be illustrated that the OMCs structure model were assumed as perfect crystal,  
195 and structural defects, impurity, surface coarseness, pore size and pore wall thickness are ignored  
196 during the simulation calculation. According, the simulation results did not correspond with the  
197 real structure of OMCs exactly, and the model structure of OMCs still need further modification  
198 or optimization for the purpose of obtaining more accurate simulation results in subsequent  
199 research. This work deepened the understanding of the adsorption state of naphthalene for OMCs  
200 on mesoscopic level. It also demonstrated that the GCMC method is effective for studying the  
201 adsorption process and gives useful guidance on research of structure-activity relationship and  
202 performance prediction of the carbon material.

203

## 204 **ACKNOWLEDGMENTS**

205 This work was financially supported by Science and Technology Planning Project of Guang

206 Dong Province of China (No. 2014A020216052) and Science and Technology Innovation Fund  
207 of Foshan City of of Guang Dong Province of China (No. 2015AG100242).  
208

## 209 REFERENCES

- 210 Allen M. P., Tildesley D. J. (1987). *Molecular Simulation of Liquids*, Oxford University Press,  
211 Oxford, UK.
- 212 Chen, L.R., Hou, T.J., Li, Y.Y., Xu, X.J. (2000). Adsorption properties of benzene in sodium-Y  
213 zeolite by Monte Carlo simulation. *Comput. Appl. Chem.* 17(1): 45-46.
- 214 Cheng, W.H. (2008). Adsorption Characteristics of Granular Activated Carbon and SPME  
215 Indication of VOCs Breakthrough. *Aerosol Air Qual. Res.* 8:178-187.
- 216 Dachs, J., Eisenreich, S.J. (2000). Adsorption onto Aerosol Soot Carbon Dominates Gas-Particle  
217 Partitioning of Polycyclic Aromatic Hydrocarbons. *Environ. Sci. Technol.* 34:3690-3697.
- 218 Evaluation and Estimation of Potential Carcinogenic Risks of PAH: Carcinogen Assessment  
219 Group; Office of Health and Environmental Assessment, Office of Research and  
220 Development, U.S. EPA: Washington, DC, 1985.
- 221 Fan, F.X., Zhang, M.J., Peng, Z.B., Chen, J., Su, M.X., Moghtaderi, B., Doroodchi, E. (2017).  
222 Direct Simulation Monte Carlo Method for Acoustic Agglomeration under Standing Wave  
223 Condition. *Aerosol Air Qual. Res.* In Press.
- 224 Febrianto, J., Kosasih, A.N., Sunarso, J.(2009). Equilibrium and kinetic studies in adsorption of  
225 heavy metals using biosorbent: a summary of recent studies. *J. Hazard. Mater.* 162: 616-645.
- 226 Galo, J., de, A.A., Soler, G.J., Sanchez, C., Lebeau, B., Patarin, J. (2002). Chemical Strategies to  
227 Design Textured Silica and Metal Oxide-Based Organised Networks: From Nanostructured  
228 Networks to Hierarchical Structures. *Chem. Rev.* 102: 4093-4138.
- 229 Gerde, P., Scholander, P. (1989). Adsorption of Polycyclic Aromatic Hydrocarbons on to Asbestos  
230 and Man-Made Mineral Fibres in the Gas Phase. IARC Scientific: Lyon, France, 140.
- 231 Guo, Z., Zhu, G., Gao, B., Zhang, D., Tian, G, Chen, Y. (2005). Adsorption of vitamin B12 on  
232 ordered mesoporous carbons coated with PMMA. *Carbon* 43(11) :2344-2351.
- 233 Hart, K.M., Pankow, J.F. (1994). High-Volume Air Sampler for Particle and Gas Sampling.2.Use  
234 of Backup Filters To Correct for the Adsorption of Gas-Phase Polycyclic Aromatic



235 Hydrocarbons to the Front Filter. *Environ. Sci. Technol.* 28: 655-661.

236 Hylland, K. (2006). Polycyclic Aromatic Hydrocarbon (PAH) Ecotoxicology in Marine  
237 Ecosystems. *J Toxicol Environ Health A.* 69(1-2):109-123.

238 International Agency for Research on Cancer (IARC) (1983). Polynuclear Aromatic Compounds,  
239 Part 1: Chemical Environmental and Experimental Data. Lyon, France.

240 International Energy Agency Coal Research (IEACR) (1995). Sloss, L. L.; Gardner, C. A.  
241 Sampling and Analysis of Trace Emissions from Coal-Fired Power Stations. London, U.K.

242 Lee, W.M.; Tong, H.C.; Yeh, S.Y. (1993). Partitioning model of PAHs between gaseous and  
243 particulate phases with consideration of reactivity of PAHs in an urban atmosphere. *Environ.*  
244 *Sci. Health A* 28(3): 563-583.

245 Lee, J., Kim, J., Hyeon, T. (2006). Recent Progress in the Synthesis of Porous Carbon Materials.  
246 *Adv. Mater* 18(16): 2073-2094.

247 Li, L., Song, H., Chen, X. (2006). Pore characteristics and electrochemical performance of  
248 ordered mesoporous carbons for electric double-layer capacitors. *Electrochim. Acta.* 51(26):  
249 5715-5720.

250 Liu, R. L.; Shi, Y. F.; Wan, Y. (2006). Triconstituent co-assembly to ordered mesostructured  
251 polymer-silica and carbon-silica nanocomposites and large-pore mesoporous carbons with  
252 high surface areas. *J. Am. Chem. Soc.* 128(35): 11652-11662.

253 Lu, A.H., Schüth, F. (2006). Nanocasting: A versatile strategy to create nanostructured porous  
254 materials. *Adv. Mater.* 18: 1793-1805.

255 Mastral, A.M., Callen, M.S., Murillo, R., Garcí'a, T. (1999). Polycyclic Aromatic Hydrocarbons  
256 and Organic Matter Associated to Particulate Matter Emitted from Atmospheric Fluidized  
257 Bed Coal Combustion. *Environ. Sci. Technol.* 33(18): 3177-3184.

258 Minchev, C., Huwe, H., Tsoncheva, T., Paneva, D., Dimitrov, M., Mitov, I. (2005). Iron oxide  
259 modified mesoporous carbons: Physicochemical and catalytic study. *Micropor. Mesopor.*  
260 *Mater.* 81(1): 333-341.

261 Ministry of Environment and Energy (1997). Scientific Criteria Document for Multimedia  
262 Standards Development PAH, Part 1: Hazard Identification and Dose- Response. Ontario,

263 Canada.

264 Saha, D., Deng, S.G. (2010). Adsorption equilibrium and kinetics of CO<sub>2</sub>, CH<sub>4</sub>, N<sub>2</sub>O, and NH<sub>3</sub> on  
265 ordered mesoporous carbon. *J. Colloid Interf. Sci.* 345: 402-409.

266 Saini, V.K., Andrade, M., Pinto, M.L., Carvalho, A.P., Pires., J. (2010). How the adsorption  
267 properties get changed when going from SBA-15 to its CMK-3 carbon replica. *Sep. Purif.*  
268 *Technol.* 75: 366-376.

269 Schrüth, F. (2003). Endo- and exotemplating to create high-surface-area inorganic materials.  
270 *Angew. Chem. Int. Ed.* 42(42): 3604-3622.

271 Sun, X.Y., Li, J.W., Li, Y.X., Yang, S.C., Chen, B.H. (2009). Adsorption of benzene and propylene  
272 in zeolite ZSM-5: Grand Canonical Monte Carlo simulations. *Chem. Res. Chin. Univ.* 25:  
273 377- 382.

274 Taguchi, A., Schüth, F. (2005). Ordered mesoporous materials in catalysis. *Micropor. Mesopor.*  
275 *Mater.* 77: 1-45.

276 Trick, K.A., Saliba, T.E. (1995). Mechanisms of the pyrolysis of phenolic resin in a carbon/  
277 phenolic composite. *Carbon* 33:1509-1515.

278 Wang, K., Huang, B., Liu, D., Ye, D. (2012). Ordered mesoporous carbons with various pore  
279 sizes: Preparation and naphthalene adsorption performance. *J. Appl. Polym. Sci.* 125(125):  
280 3368-3375.

281 Wang, K., Zhao, J., Fu, M., Zhou, G., Huang, B., Ye, D. (2013). Experimental and Molecular  
282 Simulation Study on the Preparation of Ordered Mesoporous Carbons. *Aerosol Air Qual.*  
283 *Res.* 13:1034-1044.

284 Zeng, W.T., Bai, H.L. (2016). Adsorption/Desorption Behaviors of Acetone over Micro-  
285 /Mesoporous SBA-16 Silicas Prepared from Rice Husk Agricultural Waste. *Aerosol Air*  
286 *Qual. Res.* 16:2267-2277.

287 Zhang, J.F., Burke, N., Yang, Y.X. (2012). Molecular simulation of propane adsorption in FAU  
288 zeolites. *J. Phys. Chem. C* 116: 9666-9674.

289 Zhou, L., Liu, X.U., Li, J.W., Wang, N., Wang, Z., Zhou, Y.P. (2005). Synthesis of ordered  
290 mesoporous carbon molecular sieve and its adsorption capacity for H<sub>2</sub>, N<sub>2</sub>, O<sub>2</sub>, CH<sub>4</sub> and

291 CO<sub>2</sub>. *Chem. Phys. Lett.* 413: 6-9.

292  
293  
294  
295  
296  
297  
298  
299  
300  
301  
302  
303  
304  
305  
306  
307  
308  
309  
310  
311  
312  
313  
314  
315  
316  
317  
318  
319  
320  
321  
322  
323  
324  
325  
326  
327  
328  
329  
330  
331

ACCEPTED MANUSCRIPT

Table. 1 Structure parameter of OMCs

OMCs	Mesopore size (nm)	Wall (nm)	$S_{\text{BET}}$ ( $\text{m}^2/\text{g}$ )	$V_{\text{meso}}$ ( $\text{cm}^3/\text{g}$ )
Simulation	4.0	2.3	334	0.15
Experiment	4.0	3	558	0.26

332  
333  
334  
335  
336  
337  
338  
339  
340  
341  
342  
343  
344  
345  
346  
347  
348  
349  
350  
351  
352  
353  
354  
355  
356  
357  
358  
359  
360  
361  
362  
363  
364  
365  
366  
367

ACCEPTED MANUSCRIPT

**FIGURE CAPTIONS**

368 Fig. 1. Schematic diagram of modelling process

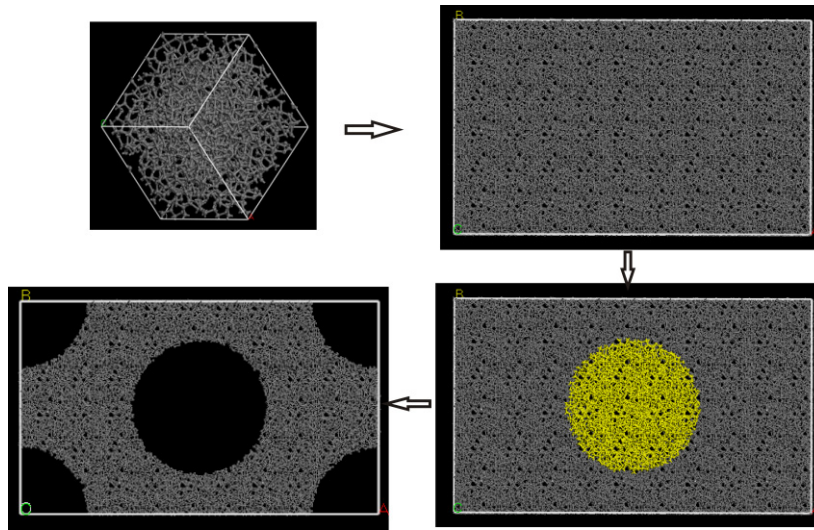


FIGURE 1

369

370

371

372

373

374

375

376

377

378

379

380

381

382

383

384

385

386

387

388

389

390

391

392

393

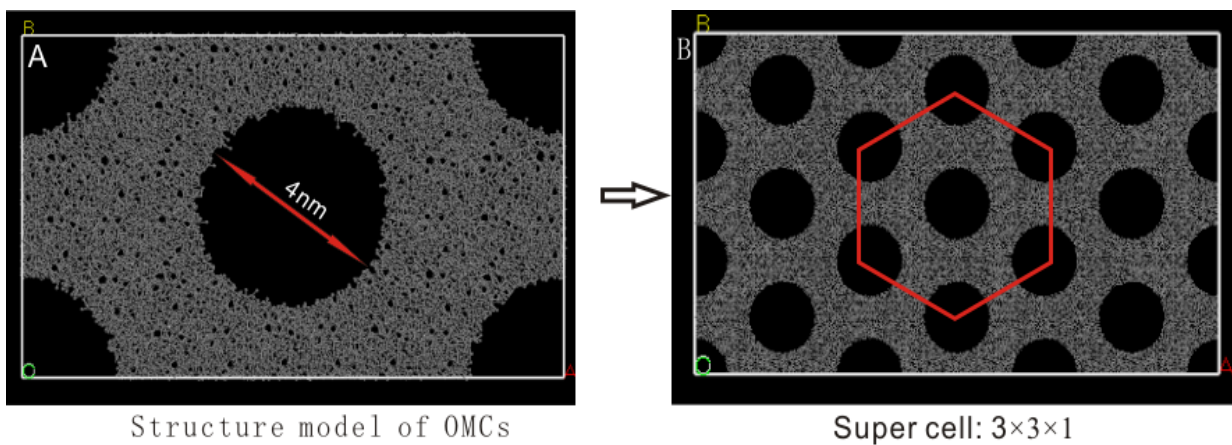
394

395

396

397

Fig. 2. Structure model of OMCs after geometry optimization (A)structure model, (B) $3 \times 3 \times 1$  supercell



398

399

400

401

402

403

404

405

406

407

408

409

410

411

412

413 Fig. 3. Accessible solvent surface area of OMCs structure model

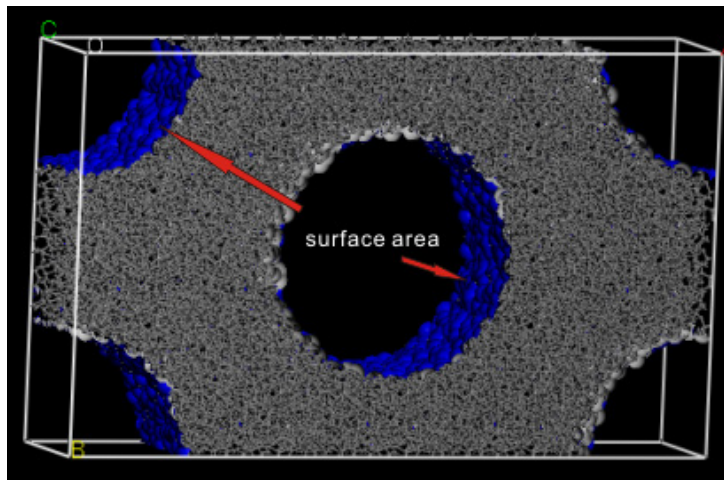


FIGURE 3

414

415

416

417

418

419

420

421

422

423

424

425

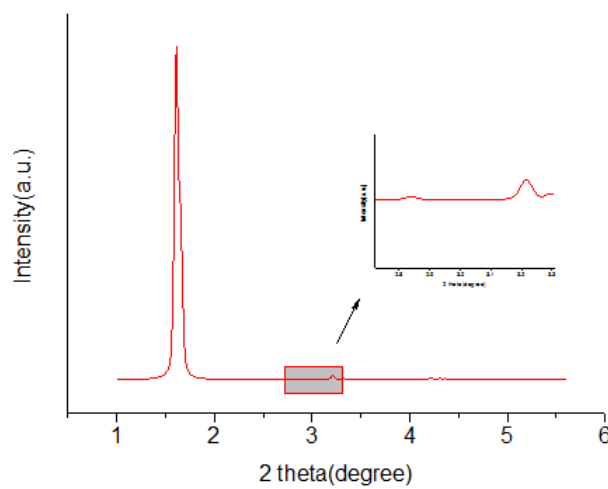
426

427

428

429

430 Fig. 4. Simulated small-angle X-ray diffraction pattern of OMCs



431

432

433

434

435

436

437

438

439

440

441

442

443

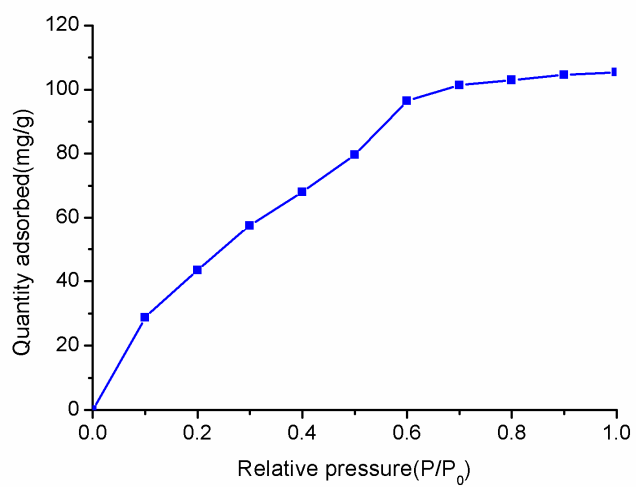
444

445

FIGURE 4



446 Fig. 5. Adsorption isotherm of naphthalene in OMCs model



447

448

FIGURE 5

449

450

451

452

453

454

455

456

457

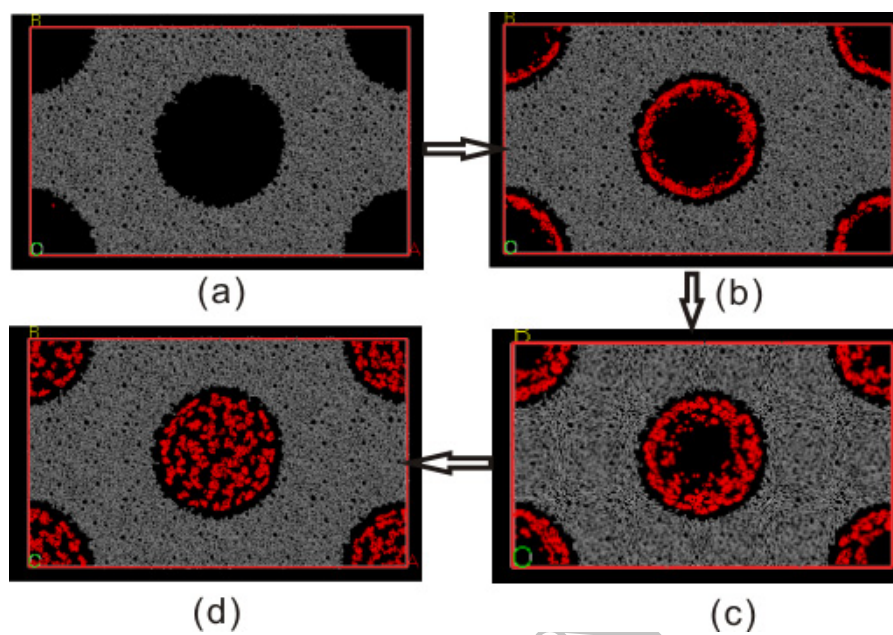
458

459

460

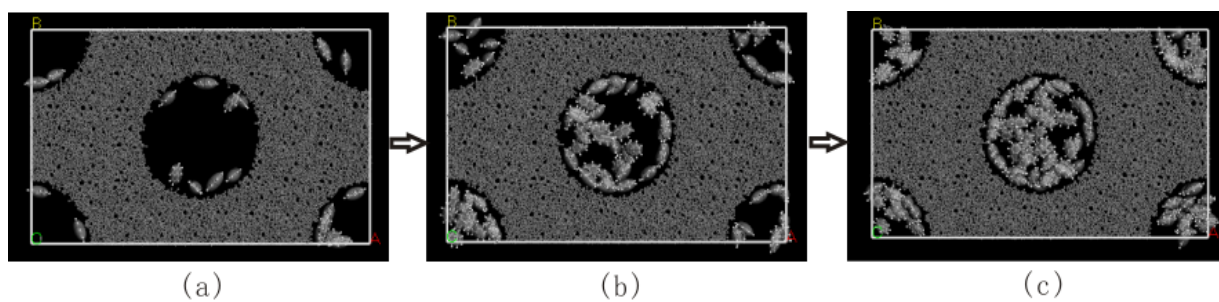
461

462 Fig. 6. Density distribution of naphthalene molecules in the OMCs model at different relative  
463 pressure: (a)  $p/p_0=0$ , (b)  $p/p_0=0.2$ , (c)  $p/p_0=0.6$ , (d)  $p/p_0=1.0$



464  
465 FIGURE 6  
466  
467  
468  
469  
470  
471  
472  
473  
474  
475  
476

477 Fig. 7. Adsorption state of naphthalene molecules in OMCs model



478

479

FIGURE 7

ACCEPTED MANUSCRIPT